The use of Raman microscopy to determine and localize vitamin E in biological samples

J. Renwick Beattie,* Ciaran Maguire,* Sarah Gilchrist,† Lindsay J. Barrett,* Carroll E. Cross,§ Fred Possmayer,‖ Madeleine Ennis,† J. Stuart Elborn,† W. James Curry,‡ John J. McGarvey,* and Bettina C. Schock†,§,1

Queen's University Belfast, Schools of *Chemistry and Chemical Engineering, †Medicine and Dentistry, ‡School of Biomedical Science, Belfast, UK; §University of California at Davis, Davis, California, USA; ‖Departments of Ob/Gyn and Biochemistry, University of Western Ontario, London, Ontario, Canada

ABSTRACT **Alpha-tocopherol (aT), the predominant form of vitamin E in mammals, is thought to prevent oxidation of polyunsaturated fatty acids. In the lung, aT is perceived to be accumulated in alveolar type II cells and secreted together with surfactant into the epithelial lining fluid. Conventionally, determination of aT and related compounds requires extraction with organic solvents. This study describes a new method to determine and image the distribution of aT and related compounds within cells and tissue sections using the light-scattering technique of Raman microscopy to enable high spatial as well as spectral resolution. This study compared the nondestructive analysis by Raman microscopy of vitamin E, in particular aT, in biological samples with data obtained using conventional HPLC analysis. Raman spectra were acquired at spatial resolutions of 2–0.8 μm. Multivariate analysis techniques were used for analyses and construction of corresponding maps showing the distribution of aT, alpha-tocopherol quinone (aTQ), and other constituents (hemes, proteins, DNA, and surfactant lipids). A combination of images enabled identification of colocalized constituents (heme/aTQ and aT/surfactant lipids). Our data demonstrate the ability of Raman microscopy to discriminate between different tocopherols and oxidation products in biological specimens without sample destruction. By enabling the visualization of lipid-protein interactions, Raman microscopy offers a novel method of investigating biological characterization of lipid-soluble compounds, including those that may be embedded in biological membranes such as aT. Beattie J. R., Maguire C., Gilchrist S., Barrett L. J., Cross C. E., Possmayer F., Ennis M., Elborn J. S., Curry W. J., McGarvey J. J., Schock B. C. The use of Raman microscopy to determine and localize vitamin E in biological samples *FASEB J.* 21, 766–776 (2007)**

Key Words · alpha-tocopherol · tissue distribution · lung tissue · Raman mapping

Alpha-tocopherol (aT) is the predominant form of vitamin E in mammals and while it has other nonantioxidant functions (1), its importance originates from its radical scavenging activity: the chromanol ring reacts with lipid peroxyl radicals to form an oxidized α-tocopheroxyl free radical, thereby inhibiting the propagation of those radicals and stabilizing polyunsaturated fatty acids in lipoproteins and cell membranes (2, 3). aT has been implemented as a protective factor in various cardiovascular- and age-related diseases as well as inflammation (2–4). Exposure to inhaled toxicants, such as cigarette smoke or ozone and the subsequent inflammatory response, have been implicated in the development of chronic lung disease function (5–10). Epidemiological evidence suggests that aT concentrations/intake may affect respiratory health and lung function (5–9). The bronchial alveolar lining (BAL) fluid of smokers contains less aT compared with nonsmokers (11), which may not be compensated for by an increase in plasma turnover of aT (12). This relative aT deficiency may render the lungs more susceptible to oxidative stress (13). However, information about the function and localization of aT in the lung is sparse. In the lung, aT concentrations are tightly regulated through active uptake and secretion by alveolar type II cells (14–16), and at the air-liquid interface aT is thought to act as the first line of defense against inhaled reactive oxygen species (ROS) and may protect surfactant lipids from peroxidation (17–19).

Generally, identification of aT in biological samples involves the extraction of lipid-soluble compounds with organic solvents (20, 21) and the addition of antioxidants (*e.g.*, butylated hydroxytoluene or ascorbic acid) may prevent oxidation during processing. aT and other tocopherols are most commonly analyzed using HPLC with fluorescence, UV, or electrochemical detection (22, 23). The concentrations of metabolites, nitration, or oxidation products, together with aT may, add valuable information about the redox balance in biological samples, but their determination mostly re-

[1] Correspondence: Queen's University Belfast, Respiratory Research Group, Department of Medicine, Grosvenor Rd., Belfast, BT12 6BJ UK. E-mail: b.schock@qub.ac.uk

doi: 10.1096/fj.06-7028com

0892-6638/07/0021-0766 © FASEB

quires separate analyses (24, 25). Furthermore, the determination of the concentration of aT in specific cells or cell fractions (e.g., organelles, mitochondria, chromatin) has yielded important information about subcellular distribution of aT (26–28). However, it is important to note that these methods require stringent and laborious isolation procedures.

Raman spectroscopy analyses the inelastic scattering of photons caused by changes in the vibrational energy of a molecule after excitation with monochromatic (laser) light. The light scattered from the sample is collected and separated into different energies, giving a Raman spectrum. The use of Raman spectroscopy offers several advantages for the analyses of biological samples. Of those, most notable are the weak Raman scattering from water, the high information content, and the nondestructive nature of the analyses. Raman spectroscopy has consequently been used to investigate a range of tissues both *in vitro* and *in vivo* (29–31). The combination of Raman spectroscopy with optical microscopy offers the possibility of acquiring extremely detailed chemical, physical, and biochemical data on a micrometer scale of spatial resolution, without lengthy sample processing and/or the addition of (bio)chemicals. A range of multivariate analysis methods can be employed to extract information, including data reduction techniques such as principal component analysis (PCA), regression methods such as partial least squares (PLS), and classification routines such as discriminant analysis (DA).

Raman spectroscopic techniques have been used to quantify various compounds in biological samples, rapidly providing high-resolution information about multiple components such as lipids, proteins, carbohydrates, and vitamins (32–34). The primary purpose of the present study was to use Raman spectroscopy combined with optical microscopy, *i.e.*, Raman microscopy to evaluate the feasibility of identifying and mapping aT in cells and tissue sections and to compare such data with those obtained following HPLC analysis. To our knowledge, the present study is the first to employ Raman microscopy either to analyze aT or to map its distribution in biological samples.

MATERIALS AND METHODS

Materials

Tocopherols and cytochrome *c* were obtained from Sigma (St. Louis, MO, USA) (DL-all-rac-α-tocopherol {T-3251}, RRR-γ-tocopherol {T-1782}, horse heart cytochrome *c* {C-7150}). Alpha-tocopherol quinone was from USBiologicals (Cleveland, OH, USA). Bovine Lung Extract Surfactant (BLES™), a commercially available pulmonary surfactant, was a gift from BLES Biochemicals Inc., London, Ontario, Canada.

Tissue preparation

C57BL6 mice (male, ~12 wk, $n=3$) were housed at 20°C and 60–70% humidity on a 12 h light/dark schedule and had access to food and water *ad libitum*. The diet contained 115 mg/kg aT (#2019, Harlan Teklad, Oxon, UK). Mice were deeply anesthetized by CO_2 inhalation before excision of lung tissue. For Raman maps of lung tissue, the lungs were perfused with PBS (PBS, without Mg^{2+}/Ca^{2+}, pH 7.4) through the pulmonary artery, until the tissue was visibly free of blood; the trachea was cannulated and the organ perfused with 4% paraformaldehyde (PFA) in PBS, pH 7.4. The lung was resected and immersion-fixed in 4% PFA (18 h, 4°C). The PFA was decanted and cryoprotected initially by immersion in 5% (w/v) sucrose/PBS (24 h, 4°C) and finally in 30% (w/v) sucrose/PBS containing 0.01% (w/v) sodium azide. All procedures were performed under the guidelines of the UK Animals (Scientific Procedures, London, UK) Act 1986.

Mouse lung tissue ($n=3$) was embedded in Jung tissue freezing medium (Leica, Wetzlar, Germany) and tissue cryosections (–25°C, 8 μm, Shandon, Runcorn, UK) were prepared. Sections were immediately transferred onto gelatin (1%)-coated CaF_2 microscope slides (UV grade polished, Crystran Ltd, Dorset, UK), air-dried, and kept in the dark and 4°C before Raman analyses. The Raman maps were acquired within 2 h of preparation without and under a flow of nitrogen, which was controlled using a Linkam LNP gas-flow controller in manual mode at the lowest setting. Raman signals were recorded initially at 2 μm spacing to obtain a low-resolution overview of the section, with subsequent mapping at 0.8 μm spacing to allow more detailed information to be recorded.

Uptake and intracellular distribution of alpha-tocopherol in A549 cells

For the calibration studies, A549 cells (adenocarcinoma, alveolar type-II-like cells, American Type Tissue Culture, Manassas, VA, USA) were cultured in 6-well plates in Dulbecco's modified Eagle medium (DMEM) (DMEM, Life Technologies, Inc., Strathclyde, UK) containing 5% fetal calf serum, 1% penicillin/streptomycin until they reached 60–70% confluence. Cells were then supplemented with aT (0–100 μmol/L) dissolved in ethanol, and the final concentration of ethanol in the culture medium was 0.02% (35). The medium was replaced with fresh medium containing aT, each day for 3 consecutive days, after which cells were trypsinized (trypsin 0.25%, Life Technologies, Inc.) and cell homogenates were prepared as described (36). Raman spectra were taken from one aliquot, while the second aliquot was used for aT determination by HPLC-UV. Concentrations of total protein were analyzed in the cell homogenate before extraction using the Bio-Rad DC protein assay (Bio-Rad Laboratories, Hercules, CA, USA), and the ratios were found to range from 3.6 to 24.6 nmol aT/mg protein, similar to published data (35). To calibrate the Raman method, the ratio of nmol aT/mg protein was used both from the biochemical analyses and from the Raman signal because the Raman signal in supplemented cells primarily consisted of aT and protein. To be able to express this quantification as an aT/lipid ratio, a calibration curve of increasing concentrations of aT diluted in palmitic acid methyl ester (PAME, an fatty acid derivative) was constructed. The detection limit was determined to be 4.43 nmol aT/mg fatty acid (or 1.2 nmol aT/μmol fatty acid).

To investigate the distribution of aT in cultured cells, A549 cells were cultured in parallel on glass coverslips immersed in the culture medium and cells were supplemented with aT as described. Coverslips were mounted on a microscope slide, and cells were fixed with 4% paraformaldehyde in PBS for 30 min. Slides were then immersed in 5% sucrose (in PBS) for 1–2 h and stored in 30% sucrose (0.01% sodium azide) at 4°C until analysis by Raman microscopy (up to 2 d). Prior to

Raman mapping the sucrose was rinsed off with distilled water, and the slide was air-dried. Raman maps were acquired at 1.5 μm spacing, and the calibration obtained from cell homogenates was employed to predict aT levels at each data point, which was then used to construct Raman maps showing the distribution of aT in A549 cells.

Stability of the Raman signal

The stability of the Raman signal of A549 cells with time was investigated by repeating the mapping of single cells (n=3) over a series of 2 h time cycles over a total period of 44 h. PCA was used to determine all the variation within the data set, while PLSDA was used to determine any variations that might have occurred over time. PLS regression was used to predict the aT concentration for each time cycle to determine any changes that might occur in the predicted aT level over time.

Oxidative stress studies

The effect of oxidation of aT on the Raman spectrum was studied by exposing aT supplemented A549 cells to H_2O_2. Briefly, cells were grown on glass coverslips and supplemented with zero or 50 μM aT for 3 d. Cells were washed with prewarmed PBS and then exposed to 200 μM H_2O_2 in serum-free medium for 2 h. In parallel, lipids were extracted from cell homogenates as described before and the concentrations of aTQ were determined by HPLC, with electrochemical detection (23).

Raman analysis

Raman spectra were recorded using a Horiba Jobin-Yvon LabRam HR800 Raman microscope, with 633 nm (20 mW at sample point) excitation, and a 300 groove mm^{-1} diffraction grating giving 12 cm^{-1} spectral resolution. A ×100 objective (Olympus M-plan NA=0.9) was used to focus the laser (confocal hole 600 μm), with a 0.1 μm step *x-y-z* stage. All optical and spectral images were recorded and processed using Labspec™ (Jobin-Yvon, Villeneuve d'Ascq, France). The diameter of the sampled area was calculated at 0.8 μm by recording a line over a vertical edge of silicon and measuring the distance required for a drop of 95% of the signal intensity. The Raman spectra were acquired between 200–1800 cm^{-1} and 2600–3600 cm^{-1} for the homogenates and intact A549 cells and 965–3030 cm^{-1} for the lung tissue sections.

Spectra from cell homogenates and intact A549 cells were brought to baseline by subtracting a linear function before being normalized to the area between 2900 and 2950 cm^{-1}. The absolute signal intensity of Raman spectroscopic bands is inherently difficult to reproduce, *e.g.*, due to the lack of reference beams as employed in absorption-based spectroscopies, and typically an internal standard is used to enable fully quantitative analysis. In this study we employed the main protein band approximating to 2930 cm^{-1}. Tissue spectra were not subjected to any processing. No consistent internal standard is in place when mapping inhomogeneous sections, so PCA must be performed on the unnormalized spectra and the amount of aT signal can then be compared to the signal levels for various biochemical constituents found in proximity to it.

Multivariate statistical analysis

All spectra were mean-centered prior to analysis. PLS regression was carried out using the Unscrambler™ V9.6 package (Camo, Trondheim, Norway), using the "Uncertainty Test" to select the Raman shifts based on their correlation with the aT concentration. Raman maps of A549 cells were constructed by converting the PLS predictions to a color scale in Microsoft Excel™ (Microsoft Corporation, Redmond, WA, USA), PLSDA, and PCA of A549 cells were completed in Simca P8.0 (Umetrics, Umeå, Sweden), with validation by an independent test set randomly selected from the full data sets and at a confidence interval of 0.05 for group separation. PCA analysis of the lung tissue sections was also carried out using the Unscrambler V9.6 package. Raman maps of lung sections were generated by converting the scores for each PC into a red/blue color image in Labspec™ (Jobin-Yvon) and copying to Microsoft Paint™ . These were converted to two separate channels by Photoshop 5.0 LE imaging software (Adobe Systems Incorporated, San Jose, CA, USA), using levels on the red and blue channels before combining them as separate red, green, and blue channels in so-called "screen blending mode" within Photoshop.

RESULTS

Raman spectra of aT and related molecules

Figure 1 shows the Raman spectrum of pure aT, with tentative assignments of the principal bands (**Table 1**). Spectra and chemical structures of pure gamma-tocopherol (gT) and alpha-tocopherol-quinone (aTQ) enable comparison with a homologous and an oxidized form, respectively. Most of the bands shift significantly between the aT and gT homologues, and some features are unique to one or another of the homologues. Of particular interest is the pair of bands arising from the aromatic part (chromanol ring) of the molecule at 1582/1593 and 1615/1620 cm^{-1} for aT and gT, respectively, and the pair of bands at 2845 and 2865 cm^{-1}, which arises from polymethylene chains (phytyl chain). The intensity near 2925 cm^{-1} derives from a different vibration of the polymethylene chain and from methyl groups. In the aTQ spectrum the intensity at 1582 and 1615 cm^{-1} is depleted and replaced by strong bands at 1635 and 1655 cm^{-1}, which possibly arise from the C=C and C=O vibrational modes of the quinone group. The C–H stretching region (2800–3100 cm^{-1}) is not affected significantly by oxidation, although a marked increase was noted in the intensity ratio of the 2920 cm^{-1} methyl/phytyl band to the phytyl-only band at 2865 cm^{-1}.

Figure 2 shows the Raman spectrum of aT within a biological matrix. Figure 2*A* and *B* compares the signal obtained from A549 cells containing a high level of aT (supplemented with 100 μM aT giving 24.6 nmol/mg protein) with one containing a low level of aT (supplemented with 0 μM aT giving 3.6 nmol/mg protein). Performing a scaled subtraction of the low aT spectrum from the high aT spectrum revealed the spectrum of aT (Fig. 2*C*) as it would be in the presence of biological molecules. The loss of many of the sharp bands that occur within pure aT (see Fig. 1*A*) and significant position shifts such as the phytyl bands shifting to 2855 and 2890 cm^{-1} from the positions observed in the pure aT (*2845* and 2865 cm^{-1}, Fig. 1) are indicative of an

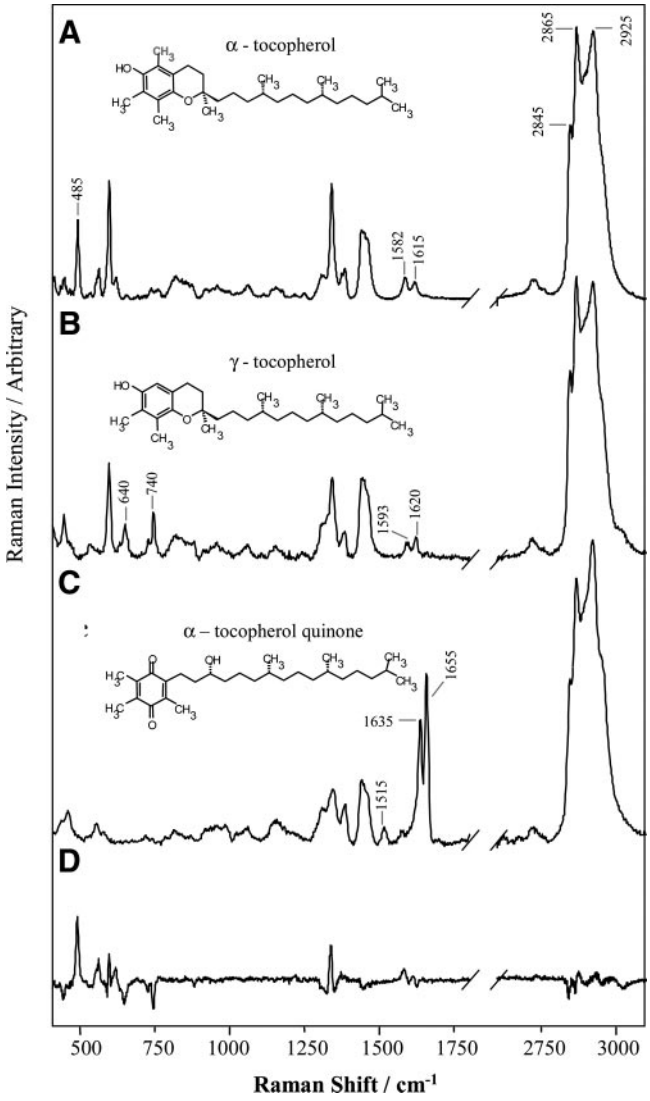

Figure 1. Raman spectra of pure tocopherols. *A)* alpha-tocopherol {aT}, (*B*) gamma-tocopherol {gT}, and (*C*) alpha-tocopherol quinone {aTQ}. Also shown is the subtraction of the gT spectrum from that of aT (*D*). No detectable bands were observed between 1800 and 2700 cm^{-1}, so this region has been excluded for clarity. Important bands are highlighted, see text for details. The extra methyl group in aT is highlighted in red. Chemical structures included for reference.

interaction with another biomolecule. For example, similar types of changes have been observed in the Raman signals of lipid molecules associated with proteins in artificial membranes (37).

Calibration

Cultured alveolar epithelial cells (A549) cells, supplemented with different concentrations of aT for 3 days, were employed to generate a reference standard of cellular aT concentrations (see Materials and Methods). As expected, the determination of aT in cell homogenates (HPLC-UV) showed a strong correlation between added aT and the concentration found within cells (R^2=0.965). Raman microscopy in conjunction with PLS regression analysis enables modeling of the concentration of aT in A549 cells supplemented with various concentrations of aT (R^2_{val}=0.954, Fig. 2, insert). Based on signal level required to exceed three times the noise level of the spectra, we could achieve a detection limit of 1.98 nmol/mg protein. Using a calibration curve of increasing concentrations of aT diluted in palmitic acid methyl ester, the detection limit was found to be 4.43 nmol aT/mg fatty acid (or 1.2 nmol aT/μmol fatty acid). The PLS regression coefficients used to predict the aT/protein ratio (Fig. 2*E*) had positive correlations at Raman shifts, which matched regions where the aT spectrum was significantly stronger than protein spectra. Conversely, the data points are negatively correlated where protein spectra are significantly stronger than the aT spectrum. This pattern of correlation demonstrates the appropriateness of the Raman shifts selected by the "Uncertainty Test" (See Materials and Methods, above).

Stability of the aT signal

To determine the robustness of the Raman signal from aT under the acquisition conditions employed, a number of time course studies were completed using pure aT (data not shown) and aT-supplemented cells. All studies were performed in a darkened room so that the only significant visible light striking the sample was the 633 nm radiation from the laser. Due to the mapping being carried out with a lateral spacing greater than the laser beam diameter, any point analyzed on the sample would only be exposed to the laser light for a total of 40 s during the entire data acquisition. A single cell was mapped over a total period of 44 h, and the Raman signal was recorded every 2 h. **Figure 3*A*** shows the PCA score plot summarizing the main variation in the Raman signals. Each time cycle is represented in a different color showing that the variation with time is insignificant compared with the variation with location. Partial PLSDA did not reveal any significant discriminant function between time cycles (P>0.05), and the aT content predicted from the PLS regression calibration showed no significant correlation with time (R^2=0.06), indicating that the intracellular aT signal in PFA fixed cells was stable over the whole acquisition period.

Oxidative stress studies: Raman spectra of aTQ

To confirm the sensitivity of Raman microscopy as a probe of aT oxidation, A549 cells were exposed to 200 μM H_2O_2, oxidizing aT to aTQ (see Methods). Using PLSDA, (Fig. 3*B*) a significant difference between the exposed and unexposed cells was observed. The Raman signal arising from the tocopherol-related compound in H_2O_2 treated cells (Fig. 2*D*, H_2O_2-treated cell signal subtracted from cellular aT signal) showed a very significant shift in the aromatic bands from 1575–1600 cm^{-1} in the untreated cells (Fig. 2*A*) to 1652 cm^{-1} in the

TABLE 1. *Selected band assignments for the Raman spectra of protein (P), fatty acid based lipids (F), alpha-tocopherol (T), and alpha-tocopherol quinone (Q) (adapted from 55, 56)*

Band position	Assignment and comments	Species
2925	CH stretch (CH_3)	P,F,T,Q
2867	CH stretch (CH_2, polymethylene chain)	F,T,Q
2847	CH stretch (CH_2, polymethylene chain)	F,T,Q
1640–1685	Amide I–COONH. Sensitive to secondary structure	P
1635–55	C = O/C = C	F,Q
1607–15	Phe and Tyr, Aromatic	P,T
1582–7	Phe and Arg, Aromatic	P,T
1450	CH_2 scissor. Decreases with increasing hydrophobicity.	P,F,T
1400	COO^- stretch for Asp + Glu.	P
1380	CH_3 twist	T,Q
1300	CH_2 twist	P,F,T,Q
1225–1305	Amide III—sensitive to secondary and tertiary structure	P
1270	= C-H deformation lipids	F
1260	His, tautomer II.	P
1214	Tyr + Phe	P
1020–1130	C-C, N stretch.	P,F,T,Q
1003	Phe ring stretch. Insensitive to environment.	P
880–965	stretching modes for terminal C-C bonds and close to *e.g.* C = O	P,F,T,Q
820–860	Tyr	P

exposed cells (Fig. 2*D*), while the intensity of the band around 2925 cm^{-1} is significantly increased relative to the phytyl bands at 2870 cm^{-1} in the oxidized sample (Fig. 2*A*). These differences are comparable with the differences observed between the spectra of pure aT and pure aTQ (Fig. 1*A*, *C*). Formation of aTQ in the cells was confirmed by HPLC-EC analyses (data not shown).

Prediction of intracellular aT distribution

Within A549 cells aT was mapped by using the Raman spectrum accumulated at each point to predict the corresponding concentrations from the regression analysis used to produce the plot in Fig. 2 (insert). **Figure 4** shows representative cells from the described supplementation studies. The progression toward red in the maps reflects an increase in aT, consistent with the average predicted aT concentration of the cells, increasing linearly with increasing supplementation (R^2=0.95 as determined by HPLC analyses).

PFA-fixed, cryoprotected mouse lung sections (8 μm) were used to investigate the distribution of aT in normal lung tissue. Initial measurements revealed a larger proportion of aTQ signal than would be expected from published data (38). Raman spectra of additional lung samples were analyzed with and without a constant flow of nitrogen over the surface. These data are consistent with the formation of aTQ (Figs. 1 and 2), under the latter conditions. Repeated measurements (over 24 h) with nitrogen flush revealed no appreciable oxidation of aT.

Figure 5 shows representative data collected from a nitrogen flushed mouse lung section obtained after hematoxylin/eosin staining (Fig. 5*A*, *B*, *E*), by bright field image (Fig. 5*C*) and by Raman signal acquisition (Fig. 5*D*, *F–J*). Additionally to identifying absolute aT, the Raman signals identified by the PCA closely match the reference spectra, confirming their assignment to DNA/protein, surfactant, and heme-containing protein signals (**Fig. 6**). Figure 5*D* shows the low-resolution Raman map (2 μm spacing) combining signals for aT, protein/DNA, and heme-containing proteins within the section. A number of highly localized aT "hotspots" are observed (white arrows). In the upper part of the section the two aT "hotspots" are scattered over a relatively wide area. The corresponding H+E stain (Fig. 5*B*) suggests that aT occurs in the capillaries, which also show high heme signals. In contrast, the aT "hotspots" in the lower half of the image are highly localized in two distinct cells (Fig. 5*D*). Figure 5*F–J* represents higher-resolution Raman maps (0.8 μm spacing) of the highlighted area (blue rectangle), showing the distribution of (Fig. 5*F*) aT, heme-containing proteins and protein/DNA (Fig. 5*G*), aTQ and heme-containing proteins, (Fig. 5*H*) aT and gT, and (Fig. 5*I*) surfactant lipids. Overlaying the heme and aTQ signals (Fig. 5*G*) reveals that all signals arising from the aTQ are found overlapping with or in close proximity to heme-containing proteins. However, it is also notable that surfactant-positive cells contain very little aTQ. In contrast to aTQ, the aT (unoxidized) signal is found more distant from the heme signals (Fig. 5*F*). Furthermore, the aT signals spread over a wider area of the cells than the aTQ signals, and comparison of the most intense regions for each molecule shows that the aT signal is 2.4 times more intense than the aTQ signal. Using the PLS regression model obtained from supplemented A549 cells, the concentration of aT in the aT positive cell is predicted to be 17.7 nmol/mg protein (or 555 nmol/mg palmitic acid). Of particular interest, the aT positive cells (Fig. 5*H*) also contain significant levels of surfactant lipids (Fig. 5*I*). To inves-

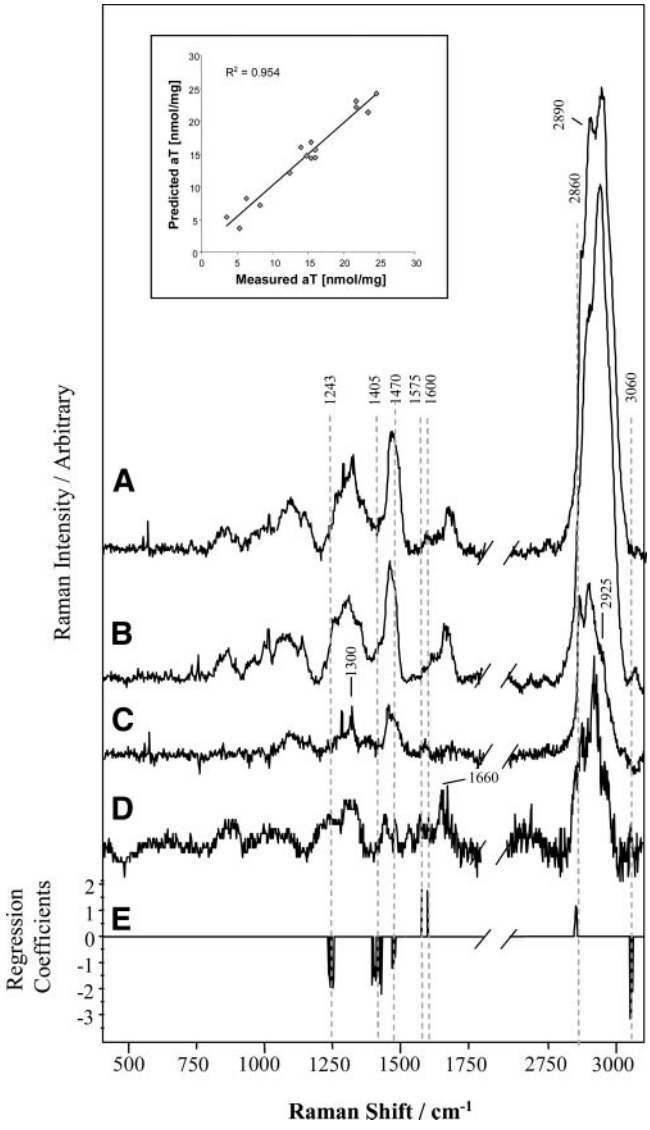

Figure 2. Raman spectra of intracellular tocopherols. Comparison of the Raman spectra for A549 cell homogenate containing (*A*) 24.6 μM and (*B*) 3.6 μM aT. The subtraction spectrum (*C*), scaled so that no negative bands appeared in the spectrum, shows the spectral signal that can be attributed to aT in the homogenate. *D)* The subtraction of the Raman signal of untreated from H_2O_2-treated A549 cells, with a clear band appearing at 1660 cm^{-1} attributable to a quinone ring. Also shown are the PLS regression coefficients (*E*) used to predict the concentration of aT from the Raman spectrum. The insert shows the correlation plot of the aT content in cell homogenates predicted using Raman spectroscopy in conjunction with PLS regression analysis against the HPLC measured concentration of aT within the homogenates. The concentration of aT within the A549 cell homogenates was controlled by supplementation of the growing cells with different concentrations of aT. The prediction correlation for aT was $R^2 = 0.954$. One representative spectrum out of five different experiments is shown.

tigate this further, we acquired a Raman spectrum of pulmonary surfactant (bovine lung extract surfactant, BLES™, Fig. 6*B*), which was consistent with the lipid spectrum in the lung section (Fig. 6*A*). For example, the ratio of the bands at 1660 and 1440 cm^{-1} is indicative of the degree of unsaturation of fatty acid lipids (39). Analysis of lung tissue detected a quite low ratio of these bands (0.171), which was comparable to the value observed in the Raman spectrum of the extracted pulmonary surfactant BLES™ (0.167). Based on published calibrations (39), this band ratio corresponds to four times more saturation than pure palmitoleic acid (16 carbons, 1 olefinic bond), suggesting that surfactant phospholipids are highly saturated. Indeed, pulmonary surfactant (BLES™) contains almost 80% saturated palmitic acid. Figure 5*J* combines the aT signal in Fig. 5*H* and surfactant image (Fig. 5*I*) with the distribution of heme-containing proteins.

DISCUSSION

This study introduces a new comprehensive method for the direct identification and localization of tocopherols and related lipophilic compounds in complex biological samples, *e.g.*, tissue sections. Analyses of the spectral

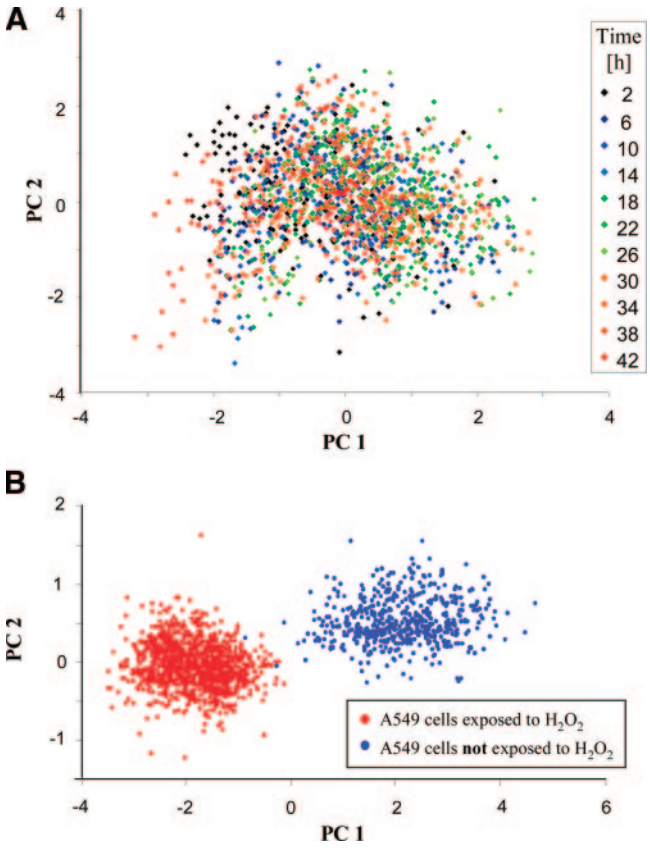

Figure 3. Stability of the Raman signal with respect to time and oxidation. *A)* PCA score plots derived from Raman spectra acquired from a single A549 cell over time. No significant variation was observed for 2 h cycles over a total time period of 44 h. *B)* Score plot of PLSDA comparing the variation in the Raman spectra obtained from untreated (blue) and H_2O_2-treated (red) A549 cells supplemented with 50 μM aT. The plot shows clear discrimination between unoxidized aT and oxidized aTQ within a complex biological matrix.

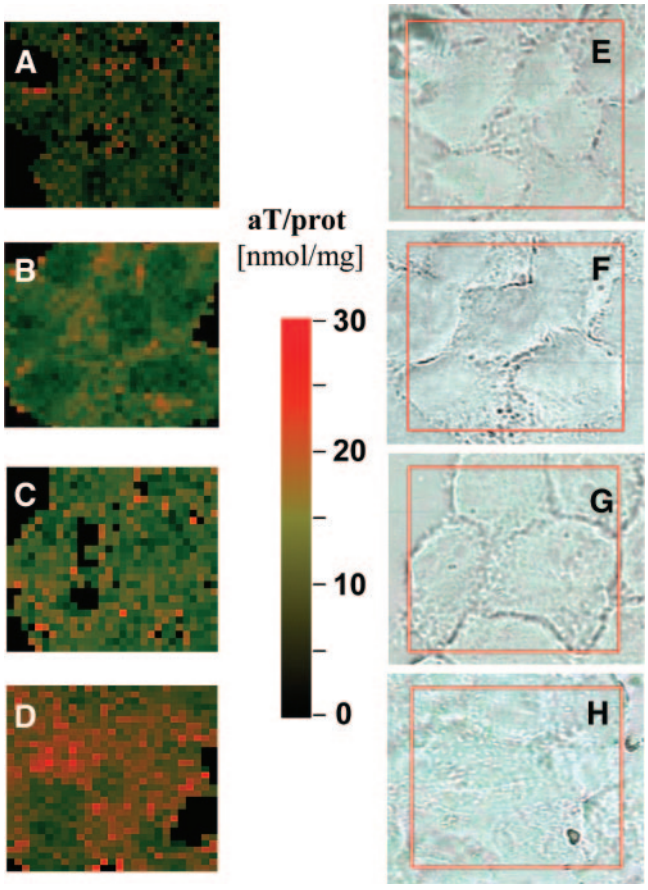

Figure 4. Raman maps of aT-supplemented A549 cells. Distribution of aT within A549 cells supplemented with a range of concentrations of aT (*A–D* are 0, 5, 25, and 50 μM). The distribution was predicted from the Raman spectra using the PLS regression model described in Fig. 2E. Increased intracellular concentrations of aT and a distinct distribution pattern were observed. The white light images of the corresponding cells are shown in (*E–H*). One representative Raman map out of five different experiments is shown.

data suggest that Raman microscopy can *a*) discriminate between different tocopherol homologues and the main oxidation product aTQ, both in pure composition and in biological environments; *b*) analyze these compounds on a single cell level and determine the localization of tocopherols within tissues at a range of spatial resolutions; *c*) provide additional information, which, in conjunction with available databases, will enable the investigation of biological material (*e.g.*, precious tissue samples) for other compounds such as heme, DNA, and lipids. If new reference compounds are required these can be included in the database.

Comparison of the Raman band assignments with the structures of the tocopherols (Fig. 1) demonstrates that all of the major bonds in the molecule are represented in the Raman spectrum. The spectral differences between the alpha- and gamma-derivatives are subtle; this is expected since the only difference between these two molecules is one methyl group. The aTQ spectrum displayed very strong bands at 1635 and 1655 cm^{-1}, tentatively assigned to the quinone ring, which is formed on a (2e-) oxidation of aT. Many of the other bands in common with aT features show frequency shifts and/or intensity changes, possibly due to conformational changes in the acyl (phytyl) tail and the consequent effect on intermolecular packing. For example the region around 1400–1500 cm^{-1} arises from CH_x modes of acyl chains and is sensitive to intermolecular forces linked to crystal packing effects. The region 1300–1350 cm^{-1}, arising from CH_2 units, is reportedly sensitive to the conformation of the acyl (phytyl) chain (39). The sensitivity of Raman signals to these various physical interactions has been used to study perturbations in a wide range of mixed systems, including protein-lipid and lipid-lipid interactions. In addition to describing a new method this paper focused on the potential aT-protein interactions (*e.g.*, with heme-containing proteins) as the lung is a highly oxidizing and metabolically active organ. Further work is underway to investigate these aT interactions in more depth using Raman microscopy.

The Raman signal in PFA fixed A549 cells over a prolonged time period showed no significant variation with time in either the signals obtained (PCA and PLSDA) or in the predicted aT concentration of the supplemented cells, indicating that the Raman signal was stable under the conditions studied. In contrast to A549 cells, the aT in tissue sections was found to be more prone to oxidation, but the introduction of a flow of nitrogen over the sample prevented oxidation even during prolonged acquisition. The oxidation rate of aT is dependant on concentration (40), section thickness/oxygen diffusion and energy of the radiation used to probe the sample. While PFA fixation may exclude any enzymatic oxidation of aT, chemical oxidation on the surface of the section (especially in the presence of iron) may still occur. Therefore, for tissue sections it is advisable to include the nitrogen flow during acquisition.

Cell homogenates with increasing concentrations of aT were used to calibrate the analyses for both the Raman signal within biological matrix and quantification of aT. We achieved a detection limit of 1.98 nmol aT/mg protein or 4.43 nmol aT/mg fatty acid (based on signal level required to exceed three times the noise level of the spectra). This appears to be similar to detection limits reported for HPLC with electrochemical detection [nmol range (22)], but mass-spectroscopy methods are more sensitive [LC-MS, pmol range (25)]. However, limits of quantification for Raman mapping would have to be assessed in the context of the spatial resolution. The compartmentalization of aT in biological tissues (*e.g.*, surfactant containing alveolar type II cells) together with two-dimensional Raman mapping may allow for a higher detection limit to be sufficient to show the distinct tissue distribution or localization of aT. In the present study we used a lateral resolution of ca. 0.8 μm. Under confocal conditions, which were not used in this work, depth profiling of samples would have been feasible in principle, possibly enabling us to identify organelles in mouse lung tissue cells. Such

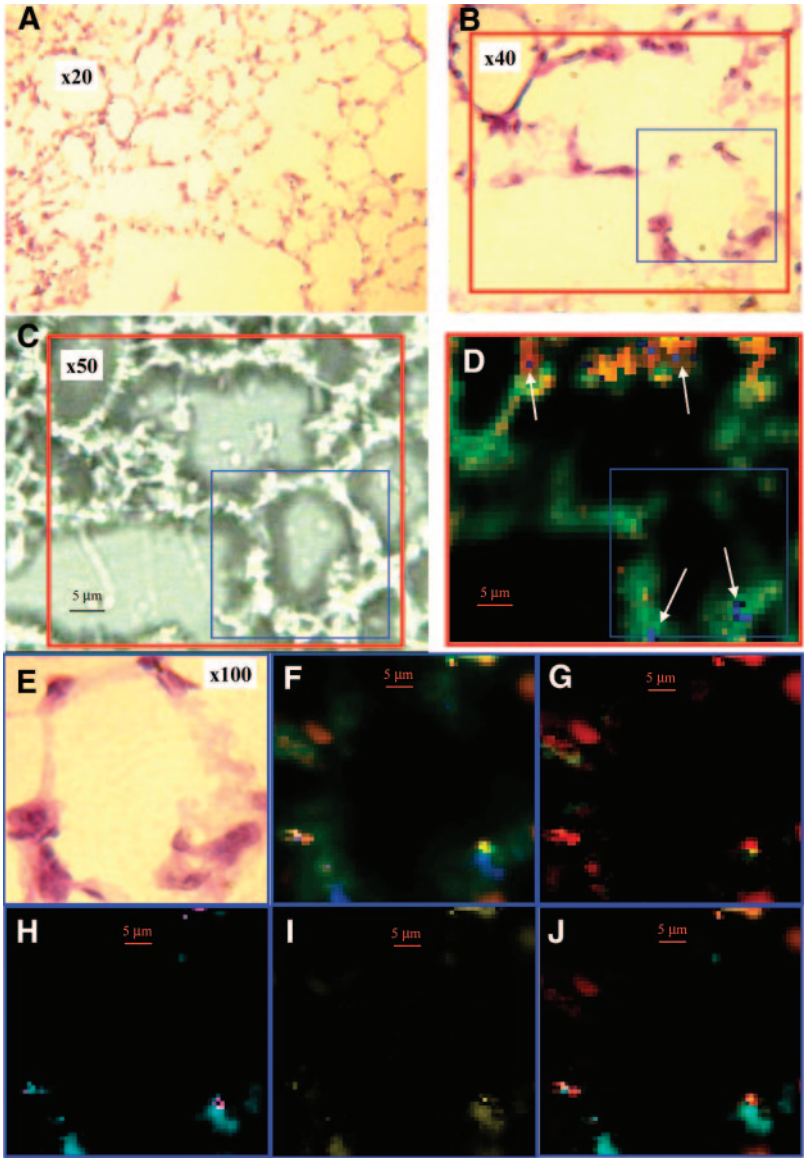

Figure 5. Raman maps of mouse lung tissue. Mouse lung (8 µm section) stained with hematoxylin/eosin (*A–E*) and unstained (*C*). The magnification is indicated in the image. The corresponding Raman images (*D*, *F–J*) show the distribution of aT in the context of other compounds (*e.g.*, protein/DNA, heme-containing proteins, and surfactant lipids). The sections were mapped using Raman microscopy (633 nm excitation, 20 s per pixel) under a nitrogen flow. PCA was used to identify the major spectral contributors in the tissue, and the PCs matching the chemical signal of aT, proteins/DNA, hemes, and surfactant lipids were converted to gray-scale channels and then combined in an RGB image. *D)* Raman map with 2 µm spacing, showing: green = protein intensity, red = heme intensity, and blue = aT intensity. Note that only a few (4 out of ~23) cells show a detectable spectral signal related to aT (white arrows). *F)* Shows the distribution of the same compounds in a higher spatial resolution (0.8 µm spacing): green = protein intensity, red = heme intensity, and blue = aT intensity. *G)* Shows the distribution of red = heme-containing proteins and green = aTQ. Note that all of the aTQ overlaps with the heme proteins, resulting in a light green to yellow color in the image. *H)* Shows the distribution of aT (cyan) and gT (magenta) and (*I*) the distribution of surfactant lipids (yellow). Image (*J*) combines the aT from image (*H*) with image (*I*) and with the distribution of heme-containing proteins (red). Shown are representative Raman maps for each spatial resolution within the lung of a single animal. In total, three lung sections derived from different animals were analyzed.

measurements might, however, be compromised by refraction effects (41). Confocal Raman microscopy has in fact been used to study chromosomes and nuclei in single cells (42, 43) and the activation of single neutrophils (43, 44). The use of confocal methods, taking appropriate account of refraction effects and possibly requiring use of immersion objectives may in the future provide additional insights into the distribution of tocopherols in membranes.

In the present study we used cells supplemented with the DL racemic form of aT and not the natural isomer (RRR-aT). Although it has been reported that all-racemic-aT and the natural RRR-aT cause similar effects with regard to human cardiovascular studies or transcriptional activity in supplemented cells (45, 46), the DL form has a lower biological activity than by the natural occurring RRR form, which may be explained by a higher affinity of the hepatic transfer protein aTTP toward the natural RRR-aT (47). The Raman signal is sensitive to interacting compounds (*e.g.*, protein, lipids), and frequency shifts may be observed, which are linked to conformational changes in the acyl (phytyl) tail and on intermolecular packing (39). The supplementary cell culture studies were used to load a cell line (A549 cells) artificially (aT dissolved in ethanol) with a range of concentrations spanning beyond typical physiological levels of aT to calibrate the Raman analyses. Although to our knowledge the specific aT-transfer protein (aTTP) is not present in A549 cells, at this point we cannot exclude that the various stereoisomers of aT may influence the Raman signal due to their differing interactions with proteins.

Imaging techniques have increased our understanding of cellular processes in recent years. For instance, fluorescent labeled aT has been successfully used to follow aT uptake into hepatic cell lines, showing not only that aT is taken up within a short time period but also tracking intracellular aT to the alpha-tocopherol transfer protein (αTTP) (48–50). However, this technique is not suitable for detecting aT already present in tissue and is limited to studies in which aT has been added *in vitro*. An antiserum raised against alpha-

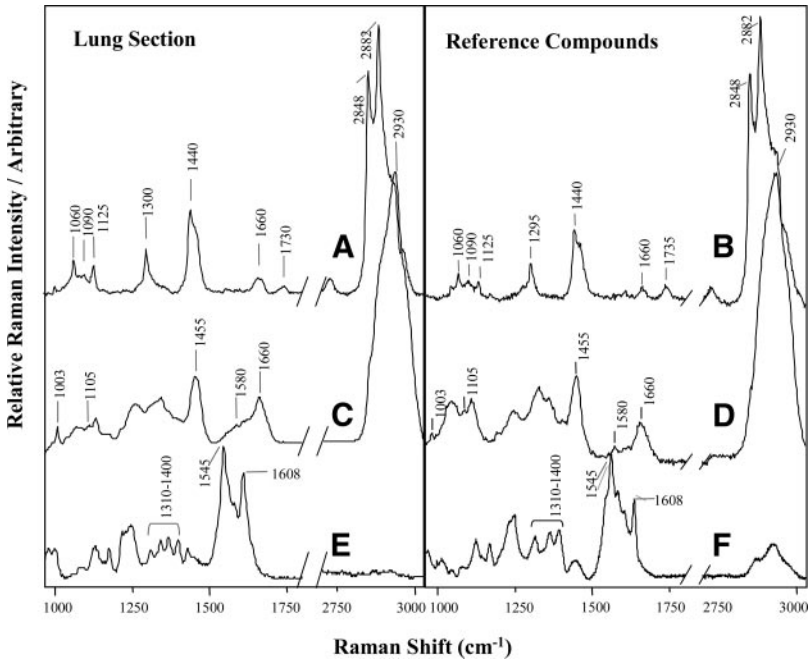

Figure 6. Comparison of Raman spectra in the lung with reference materials. Raman signals identified within the lung tissue (*A*, *C*, *E*), and the corresponding spectra of reference samples (*B*, *D*, *F*): (*A*) fatty acid, (*B*) pulmonary surfactant, BLES™, (*C*) protein and DNA, (*D*) porcine retinal nucleus (DNA) (30), (*E*) heme-containing protein, and (*F*) horse heart cytochrome *c*.

tocopherol-succinate-conjugated to BSA is commercially available (USBiologicals), but it only recognizes an aT-BSA complex. Furthermore, these two methods involve addition of synthetic biochemicals rather than enabling analysis of an unperturbed system. Raman analysis does not require addition of any biochemical agents, labels *etc.*, nor does it degrade the tissue, thereby preserving it for further analyses (51).

Recently, time-of-flight secondary ion mass spectrometry (TOF-SIMS) was used to visualize a number of lipid compounds, including vitamin E (52), achieving similar levels of spatial (*i.e.*, lateral) resolution to the present Raman method (around 1 μm). Raman can achieve a high level of specificity and spatial resolution for lipid components, with previous studies demonstrating that the fatty acid profile can be predicted from the Raman signal of a fatty acid-based lipid (32, 53). Furthermore, compared with the other methods discussed above, histological staining can be performed on the same lung section as used for Raman signal acquisition.

Moreover, Raman microscopy can distinguish not only the different tocopherol-related compounds in the presence of a complex matrix (cells), but it also provides information about matrix constituents. For example, a single scan was employed to gather all the information shown in the Raman maps (Fig. 5*F–J*), which display aT, gT, aTQ, heme-containing proteins, DNA/protein, and surfactant lipids. Using RBG images, at least three different components can be displayed simultaneously, and overlaying of the separate images adds valuable information about potential colocalization of components. This is of considerable biological interest as distinct distributions, and colocalizations may help to identify specific cells or metabolic processes. In this study a distinct distribution of aT in mouse lung tissue was demonstrated, which colocalized with pulmonary surfactant lipids. The presence of both these constituents may be used to identify the cells as alveolar type II cells, which, enriched in aT, secrete aT together with surfactant (54). We also observed a colocalization of heme-containing proteins with aTQ, suggesting that heme-containing cytochromes are responsible for some aT oxidation. However, heme-containing proteins were mainly observed in surfactant-negative cells. Furthermore, surfactant positive cells contain very little oxidized aT. There are some very small detectable "hotspots" of gT (compared to aT) in the lung section, some of which are localized in surfactant positive cells (Fig. 5*H*). Further work will apply Raman microscopy to identify the metabolic fate and removal of aT and gT in lung tissue under both normal conditions and those of oxidative stress and disease.

In summary, this study has demonstrated the capacity of Raman microscopy to map the distribution of aT and related compounds in A549 cells and lung sections. With technological advances in Raman spectroscopic methods, it is reasonable to expect that it will be possible to reduce acquisition time and spatial resolution significantly. As an imaging technique it will offer insight into complex biological processes that may help to identify further insights into the biological functions of aT, especially with regards to intracellular distributions and metabolic fate. FJ

The authors would like to thank BLES Biochemicals Inc., Ontario, Canada, for the kind gift of Bovine Lung Extract Surfactant (BLES™). Research was supported by R&D Office NI (SPI/2384/03) and NIH (ES011985). Purchase of the Raman microscope was assisted by funding from BBSRC (JREI 18471). The authors express thanks to Professor Thomas Huser, NSF Centre for Biophotonics at UC Davis, for his critical suggestions concerning the manuscript.

REFERENCES

1. Azzi, A., Ricciarelli, R., and Zingg, J. M. (2002) Non-antioxidant molecular functions of alpha-tocopherol (vitamin E). *FEBS Lett.* **519,** 8–10
2. Ingold, K. U., Webb, A. C., Witter, D., Burton, G. W., Metcalfe, T. A., and Muller, D. P. (1987) Vitamin E remains the major lipid-soluble, chain-breaking antioxidant in human plasma even in individuals suffering severe vitamin E deficiency. *Arch. Biochem. Biophys.* **259,** 224–245
3. Traber, M. G. (2005) Vitamin E. In *Modern Nutrition in Health and Disease* (Shils, M. E., Olson, J. A., Shike, M., and Ross, A. C., eds) pp. 396–411, Lippincott Williams & Wilkins, Baltimore, Maryland, USA
4. Singh, U., Devaraj, S., and Jialal, I. (2005) Vitamin E, oxidative stress, and inflammation. *Annu. Rev. Nutr.* **25,** 151–174
5. Romieu, I., and Trenga, C. (2001) Diet and obstructive lung diseases. *Epidemiol. Rev.* **23,** 268–287
6. Troisi, R. J., Willett, W. C., Weiss, S. T., Trichopoulos, D., Rosner, B., and Speizer, F. E. (1995) A prospective study of diet and adult-onset asthma. *Am. J. Respir. Crit. Care. Med.* **151,** 1401–1408
7. Tabak, C., Smit, H. A., Rasanen, L., Fidanza, F., Menotti, A., Nissinen, A., Feskens, E. J., Heederik, D., and Kromhout, D. (1999) Dietary factors and pulmonary function: a cross sectional study in middle aged men from three European countries. *Thorax* **54,** 1021–1026
8. Smit, H. A., Grievink, L., and Tabak, C. (1999) Dietary influences on chronic obstructive lung disease and asthma: a review of the epidemiological evidence. *Proc. Nutr. Soc.* **58,** 309–319
9. Pryor, W. A. (1991) Can vitamin E protect humans against the pathological effects of ozone in smog? *Am. J. Clin. Nutr.* **53,** 702–722
10. MacNee, W. (2000) Oxidants/antioxidants and COPD. *Chest* **117,** 303S–317S
11. Pacht, E. R., Kaseki, H., Mohammed, J. R., Cornwell, D. G., and Davis, W. B. (1986) Deficiency of vitamin E in the alveolar fluid of cigarette smokers. Influence on alveolar macrophage cytotoxicity. *J. Clin. Invest.* **77,** 789–796
12. Bruno, R. S., and Traber, M. G. (2006) Vitamin E biokinetics, oxidative stress and cigarette smoking. *Pathophysiology* **13,** 143–149
13. Tolle, A., Schlame, M., Charlier, N., Guthmann, F., and Rustow, B. (2005) Vitamin E differentially regulates the expression of peroxiredoxin-1 and -6 in alveolar type II cells. *Free. Radic. Biol. Med.* **38,** 1401–1408
14. Kolleck, I., Sinha, P., and Rustow, B. (2002) Vitamin E as an antioxidant of the lung: mechanisms of vitamin E delivery to alveolar type II cells. *Am. J. Respir. Crit. Care. Med.* **166,** S62–66
15. Kolleck, I., Wissel, H., Guthmann, F., Schlame, M., Sinha, P., and Rustow, B. (2002) HDL-holoparticle uptake by alveolar type II cells: effect of vitamin E status. *Am. J. Respir. Cell Mol. Biol.* **27,** 57–63
16. Sinha, P., Kolleck, I., Volk, H. D., Schlame, M., and Rustow, B. (2002) Vitamin E deficiency sensitizes alveolar type II cells for apoptosis. *Biochim. Biophys. Acta* **1583,** 91–98
17. Cross, C. E., van der Vliet, A., O'Neill, C. A., Louie, S., and Halliwell, B. (1994) Oxidants, antioxidants, and respiratory tract lining fluids. *Environ. Health. Perspect.* **102 Suppl. 10,** 185–191
18. Bouhafs, R. K., and Jarstrand, C. (1999) Phagocyte-induced lipid peroxidation of lung surfactant. *Pediatr. Pulmonol.* **27,** 322–327
19. Bouhafs, R. K., and Jarstrand, C. (1999) Lipid peroxidation of lung surfactant by bacteria. *Lung* **177,** 101–110
20. Barbas, C., Castro, M., Bonet, B., Viana, M., and Herrera, E. (1997) Simultaneous determination of vitamins A and E in rat tissues by high-performance liquid chromatography. *J. Chromatogr. A.* **778,** 415–420
21. Ito, Y., Ochiai, J., Sasaki, R., Suzuki, S., Kusuhara, Y., Morimitsu, Y., Otani, M., and Aoki, K. (1990) Serum concentrations of carotenoids, retinol, and alpha-tocopherol in healthy persons determined by high-performance liquid chromatography. *Clin. Chim. Acta* **194,** 131–144
22. Podda, M., Weber, C., Traber, M. G., and Packer, L. (1996) Simultaneous determination of tissue tocopherols, tocotrienols, ubiquinols, and ubiquinones. *J. Lipid Res.* **37,** 893–901
23. Ikenoya, S., Abe, K., Tsuda, T., Yamano, Y., Hiroshima, O., Ohmae, M., and Kawabe, K. (1979) Electrochemical detector for high-performance liquid chromatography. II. Determination of tocopherols, ubiquinones and phylloquinone in blood. *Chem. Pharm. Bull. (Tokyo)* **27,** 1237–1244
24. Galli, F., Lee, R., Dunster, C., and Kelly, F. J. (2002) Gas chromatography mass spectrometry analysis of carboxyethyl-hydroxychroman metabolites of alpha- and gamma-tocopherol in human plasma. *Free. Radic. Biol. Med.* **32,** 333–340
25. Leonard, S. W., Bruno, R. S., Paterson, E., Schock, B. C., Atkinson, J., Bray, T. M., Cross, C. E., and Traber, M. G. (2003) 5-nitro-gamma-tocopherol increases in human plasma exposed to cigarette smoke in vitro and in vivo. *Free. Radic. Biol. Med.* **35,** 1560–1567
26. Saito, Y., Yoshida, Y., Nishio, K., Hayakawa, M., and Niki, E. (2004) Characterization of cellular uptake and distribution of vitamin E. *Ann. N. Y. Acad. Sci.* **1031,** 368–375
27. Panin, L. E., Polyakov, L. M., Kolosova, N. G., Russkikh, G. S., and Poteryaeva, O. N. (1998) Distribution of tocopherol and apolipoprotein A-I immunoreactivity in rat liver chromatin. *Membr. Cell Biol.* **11,** 631–640
28. Lang, J. K., Gohil, K., and Packer, L. (1986) Simultaneous determination of tocopherols, ubiquinols, and ubiquinones in blood, plasma, tissue homogenates, and subcellular fractions. *Anal. Biochem.* **157,** 106–116
29. Min, Y. K., Yamamoto, T., Kohda, E., Ito, T., and Hamaguchi, H. (2005) 1064 nm near-infrared multichannel Raman spectroscopy of fresh human lung tissues. *J. Raman Spectrosc.* **36,** 73–76
30. Beattie, J. R., Brockbank, S., McGarvey, J. J., and Curry, W. J. (2005) Effect of excitation wavelength on the Raman spectroscopy of the porcine photoreceptor layer from the area centralis. *Mol. Vision* **11,** 825–832
31. Haka, A. S., Volynskaya, Z., Gardecki, J. A., Nazemi, J., Lyons, J., Hicks, D., Fitzmaurice, M., Dasari, R. R., Crowe, J. P., and Feld, M. S. (2006) In vivo margin assessment during partial mastectomy breast surgery using Raman spectroscopy. *Cancer Res.* **66,** 3317–3322
32. Beattie, J. R., Bell, S. E. J., Borgaard, C., Fearon, A. M., and Moss, B. W. (2004) Multivariate prediction of clarified butter composition using Raman spectroscopy. *Lipids* **39,** 897–906
33. Yang, H., and Irudayaraj, J. (2002) Rapid determination of vitamin c by NIR, MIR and FT-Raman techniques. *J. Pharm. Pharmacol.* **54,** 1247–1255
34. Celedon, A., and Aguilera, J. M. (2002) Applications of microprobe Raman spectroscopy in food science. *Food Sci. Tech. Int.* **8,** 101–108
35. Nardini, M., Finkelstein, E. I., Reddy, S., Valacchi, G., Traber, M., Cross, C. E., and van der Vliet, A. (2002) Acrolein-induced cytotoxicity in cultured human bronchial epithelial cells. Modulation by alpha-tocopherol and ascorbic acid. *Toxicology* **170,** 173–185
36. Schock, B. C., Van Der Vliet, A., Corbacho, A. M., Leonard, S. W., Finkelstein, E., Valacchi, G., Obermueller-Jevic, U., Cross, C. E., and Traber, M. G. (2004) Enhanced inflammatory responses in alpha-tocopherol transfer protein null mice. *Arch. Biochem. Biophys.* **423,** 162–169
37. Levin, I. W. (1988) Molecular reorganizations in biological-membranes—identification of lipid-lipid and lipid protein interactions by Raman spectroscopy. *Biophys. J.* **53,** A244–A244
38. Gille, L., Gregor, W., Staniek, K., and Nohl, H. (2004) Oxidized vitamin E and ubiquinone—competition for binding sites, of the mitochondrial cytochrome bc(1) complex? *Vit. E Health* **1031**, 341–343
39. Beattie, J. R., Bell, S. J., and Moss, B. W. (2004) A critical evaluation of Raman spectroscopy for the analysis of lipids: fatty acid methyl esters. *Lipids* **39,** 407–419
40. Ingold, K. U., Bowry, V. W., Stocker, R., and Walling, C. (1993) Autoxidation of lipids and antioxidation by alpha-tocopherol and ubiquinol in homogeneous solution and in aqueous dispersions of lipids: unrecognized consequences of lipid particle size as exemplified by oxidation of human low density lipoprotein. *Proc. Natl. Acad. Sci. U. S. A.* **90,** 45–49
41. Everall, N. (2000) Confocal raman microscopy: why the depth resolution and spatial accuracy can be much worse than you think. *Appl. Spectr.* **54,** 1515
42. Puppels, G. J., de Mul, F. F., Otto, C., Greve, J., Robert-Nicoud, M., Arndt-Jovin, D. J., and Jovin, T. M. (1990) Studying single

living cells and chromosomes by confocal Raman microspectroscopy. *Nature* **347,** 301–303
43. Tang, W., Newton, R. J., Xie, C. A., Li, Y. Q., and Whitley, N. (2005) Non-destructive analysis of the nuclei of transgenic living cells using laser tweezers and near-infrared Raman spectroscopic technique. *Genom. Proteom. Bioinfo.* **3,** 169–178
44. Sijtsema, N. M., Tibbe, A. G. J., Segers-Nolten, I., Verhoeven, A. J., Weening, R. S., Greve, J., and Otto, C. (2000) Intracellular reactions in single human granulocytes upon phorbol myristate acetate activation using confocal Raman microspectroscopy. *Biophys. J.* **78,** 2606–2613
45. Muller, P. Y., Netscher, T., Frank, J., Stoecklin, E., Rimbach, G., and Barella, L. (2005) Comparative quantification of pharmacodynamic parameters of chiral compounds (RRR- vs. all-rac-alpha tocopherol) by global gene expression profiling. *J. Plant. Physiol.* **162,** 811–817
46. Kraemer, K., Koch, W., and Hoppe, P. P. (2004) Is all-rac-alpha-tocopherol different from RRR-alpha-tocopherol regarding cardiovascular efficacy? A meta-analysis of clinical trials. *Ann. N. Y. Acad. Sci.* **1031,** 435–438
47. Blatt, D. H., Leonard, S. W., and Traber, M. G. (2001) Vitamin E kinetics and the function of tocopherol regulatory proteins. *Nutrition* **17,** 799–805
48. Qian, J., Wilson, K., Nava, P., Morley, S., Atkinson, J., and Manor, D. (2004) Intracellular localization of alpha-tocopherol transfer protein and alpha-tocopherol. *Ann. N. Y. Acad. Sci.* **1031,** 330–331
49. Atkinson, J. K., Nava, P., Frahm, G., Curtis, V., and Manor, D. (2004) Fluorescent tocopherols as probes of inter-vesicular transfer catalyzed by the alpha-tocopherol transfer protein. *Ann. N. Y. Acad. Sci.* **1031,** 324–327
50. Qian, J., Morley, S., Wilson, K., Nava, P., Atkinson, J., and Manor, D. (2005) Intracellular trafficking of vitamin E in hepatocytes: the role of tocopherol transfer protein. *J. Lipid Res.* **46,** 2072–82
51. Song, L., Molckovsky, A., Wang, K., Gao, T. Y., Basset, N., Cirocco, M., Marcon, N., Hsieh, E., Riddell, R., Shim, M., and Wilson, B. (2002) Raman spectroscopy for in vivo classification of Barrett's tissue. *Gastroenterology* **122,** M1372
52. Touboul, D., Brunelle, A., Halgand, F., De La Porte, S., and Laprevote, O. (2005) Lipid imaging by gold cluster time-of-flight secondary ion mass spectrometry: application to Duchenne muscular dystrophy. *J. Lipid Res.* **46,** 1388–1395
53. Beattie, J. R., Bell, S. E. J., Borgaard, C., Fearon, A., and Moss, B. W. (2006) Prediction of adipose tissue composition using Raman spectroscopy: Average properties and individual fatty acids. *Lipids* **41,** 287–294
54. Rustow, B., Haupt, R., Stevens, P. A., and Kunze, D. (1993) Type II pneumocytes secrete vitamin E together with surfactant lipids. *Am. J. Physiol.* **265,** L133–139
55. Tu, A. T. (1982) *Raman Spectroscopy in Biology: Principles and Applications*, John Wiley and Sons, Hoboken, New Jersey, USA
56. Spiro, T. G. (1986) *Biological Applications of Raman Spectroscopy* Vol. 1, John Wiley and Sons, Hoboken, New Jersey, USA

Received for publication August 13, 2006.
Accepted for publication October 11, 2006.